Speciation driven by ancestrally polymorphic chromosomal inversions

Running title: Inversions and speciation in *Drosophila*

Authors:
Poikela, N.[1], Laetsch, D. R.[2], Lohse, K.[2*], & Kankare, M[1*].
[1] Department of Biological and Environmental Science, University of Jyväskylä, Finland
[2] Institute of Evolutionary Biology, University of Edinburgh, United Kingdom
[*] these authors contributed equally

Corresponding author:
Noora Poikela, Department of Biological and Environmental Science, P.O. Box 35, FI-40014 University of Jyväskylä, Finland
E-mail: noora.p.poikela@gmail.com
Phone: +358 40 5383527

Abstract

Chromosomal inversions may play a central role in speciation through their ability to reduce recombination and therefore genetic exchange at inverted parts of the genome between diverging populations. We analysed long- and short-read whole-genome data from sympatric and allopatric populations of two *Drosophila virilis* group species, *D. montana* and *D. flavomontana*, to understand how inversions have contributed to the divergence of these sister species. Using highly contiguous genome assemblies for both species, we identified three large alternatively fixed inversions on the X chromosome and one in each of the autosomes 2L, 4 and 5. A comparison of demographic models estimated for inverted and non-inverted (colinear) chromosomal regions suggest that these inversions most likely arose before or around the time of the species split. We also detected low rate of interspecific gene flow (introgression) from *D. montana* to *D. flavomontana*, which was further reduced inside inversions and was lower in allopatric than in sympatric populations. Together these findings suggest that the inversions have reduced gene exchange between these sister taxa both before and after the onset of species divergence and that low levels of recent introgression may have led to the reinforcement of reproductive barriers previously detected between these species. Our results suggest that ancestrally polymorphic inversions may act as drivers of speciation by allowing the accumulation of divergence inside inversions, while gene flow at colinear regions continues until the evolving reproductive barriers complete speciation.

Key words: chromosomal inversion, coalescence, *Drosophila flavomontana, Drosophila montana*, genetic divergence, introgression, speciation

Introduction

Chromosomal inversions, genomic regions with reversed gene order relative to the standard form, have been detected in many species of insects, fish, birds, mammals and plants, but their frequency varies widely between and even within taxa (Stone et al. 1960; Wellenreuther and Bernatchez 2018). Inversions are suggested to be important drivers of adaptation and speciation with gene flow, as they can suppress recombination between alternate rearrangements and create associations between sets of alleles conferring local adaptation, mate choice and genetic incompatibilities (Sturtevant 1921; Butlin 2005; Hoffmann and Rieseberg 2008). While experimental evidence of inversions' effects on speciation is still scarce, genomic data from new species pairs, together with proper inference of the history of inversions and interspecific gene flow, offer a promising way to increase our understanding on the role of inversions in speciation (Faria and Navarro 2010; Faria et al. 2018).

Inversions have attracted scientists for decades, which has given rise to a wide range of theories on the role of inversions in adaptation and speciation with gene flow (reviewed in (Hoffmann and Rieseberg 2008; Faria and Navarro 2010)). A newly established inversion may be favoured by selection if it protects locally adapted allele complexes within inverted region by reducing recombination between populations with alternate rearrangements (Kirkpatrick and Barton 2006). Also, inversion breakpoints may be direct targets of selection, if they change the reading frame and/or expression patterns of genes located on these regions (Matzkin et al. 2005; Guerrero et al. 2012). Once an inversion becomes fixed between diverging lineages, it may contribute to their speciation in different ways depending on whether the populations evolve in isolation or in contact with each other. In allopatric speciation, long-term geographic isolation between populations will inevitably lead to a build-up of genetic incompatibilities as an incidental by-product of drift and selection (Seehausen et al. 2014). In secondary contact between these populations, the existing genetic incompatibilities residing within inversions will be protected, while the ones located outside of them are more susceptible to the homogenizing effects of gene flow (Noor et al. 2001). On the other hand, populations that diverge in the presence gene flow may accumulate genetic divergence and genetic incompatibilities within inversions over generations of reduced recombination on the inverted gene regions (Navarro and Barton 2003). In both scenarios, inversions harbouring incompatibilities delay species' fusion and provide time for additional barriers to emerge. For example, prezygotic reproductive barriers are expected to be reinforced in response to genetic incompatibilities and maladaptive hybridization (reinforcement) (Servedio and Noor 2003), particularly if the loci responsible for prezygotic isolation and genetic incompatibilities are located within inversions (Trickett and Butlin 1994; Butlin 2005). Two kinds of empirical observations give indirect support for these theories. First, genes maintaining local adaptation, as well as premating barriers and genetic incompatibilities between species, have often found to be located within fixed inversion differences (Noor et al. 2001; Lowry and Willis 2010; Fishman et al. 2013). And second, fixed inversions generally have elevated genetic divergence compared to colinear chromosomal regions (Noor et al. 2007; Kulathinal et al. 2009; Lohse et al. 2015).

Speciation via suppressed recombination may occur in nature if (1) closely related species carry alternatively fixed inversions, (2) inversions suppress recombination and (3) the suppression of recombination plays an important role in reproductive isolation (Faria and Navarro 2010). So far only a few studies have dissected the evolutionary history of inversions to explore their role in speciation (e.g. (Lohse et al. 2015; Fuller et al. 2018)). Demographic models can quantify the age of inversions in relation to the species' divergence time of the colinear background, and the amount of long-term effective post-divergence gene flow (introgression) inside and outside inversions (Noor and Bennett 2009). Similarly, recent or ongoing introgression can be diagnosed by comparing estimated gene flow between sympatric and allopatric population pairs (Noor and Bennett 2009). Inversions, which have fixed around or after the onset of species divergence can be favoured by selection to protect existing genetic incompatibilities from the homogenising effects of introgression, if the species live in contact with each other at some stage. On the other hand, inversions whose divergence time predates the species' split must have been in a polymorphic state in the common ancestral populations, with different frequencies

in subpopulations/lineages. These inversions may play a major role in establishing patterns of elevated genetic divergence within inversions, even without extensive gene flow occurring after the species' split (Noor and Bennett 2009; Fuller et al. 2018).

Two *Drosophila virilis* group species, *Drosophila montana* and *Drosophila flavomontana*, offer a great opportunity to investigate the role of inversions in the formation of species boundaries. Based on the polytene chromosome studies, these species have several alternatively fixed inversions (Stone et al. 1960; Throckmorton 1982), but studies on the genomic divergence of the inversions are still lacking. Species of the *montana* complex (*D. montana*, D. *flavomontana*, *D. lacicola* and *D. borealis*) have diverged ~3.8 Mya in the Rocky Mountains area (Patterson 1952; Throckmorton 1982; Hoikkala and Poikela 2022; Yusuf et al. 2022), and presently *D. montana* and *D. flavomontana* inhabit variable climates in the Rocky Mountains and the western coast of North America (Hoikkala and Poikela 2022). In the mountains, *D. montana* has spread to higher altitudes than *D. flavomontana*, while on the western coast, where *D. flavomontana* has spread relatively recently, both species live at low altitudes (Fig. 1; (Patterson 1952; Poikela et al. 2019; Hoikkala and Poikela 2022)). In both sites, populations of the two species can be regarded as sympatric or parapatric. Moreover, *D. montana* has allopatric populations on high latitudes, e.g. in Alaska, where *D. flavomontana* does not exist (Fig. 1; (Poikela et al. 2019)). *D. montana* and *D. flavomontana* have strong pre- and postzygotic barriers across their distribution range, and *D. flavomontana* also show signs of reinforcement in prezygotic barriers in sympatric populations (Poikela et al. 2019). Regardless of the strong reproductive isolation, some interspecific hybrids have been reported to be found in nature (Patterson 1952; Throckmorton 1982), and they can also be produced in the laboratory (Poikela et al. 2019).

Here, we explored whether and how inversions can contribute to speciation process, using *D. montana* and *D. flavomontana* as a model system. Long- and short-read sequencing data from allopatric and sympatric populations of the species enabled us to accurately identify the presence of alternatively fixed inversions between the species. Demographic modelling allowed us to estimate the age of these inversions and estimate their effect on the long-term rate of introgression. We asked the following questions:

(1) How many alternatively fixed inversions do *D. montana* and *D. flavomontana* carry?
(2) What are the likely ages of these inversion differences and how do they compare to the species divergence time?
(3) Have inversions contributed to the speciation process by protecting existing genetic incompatibilities in secondary contact and/or by accumulating them in the presence of gene flow?

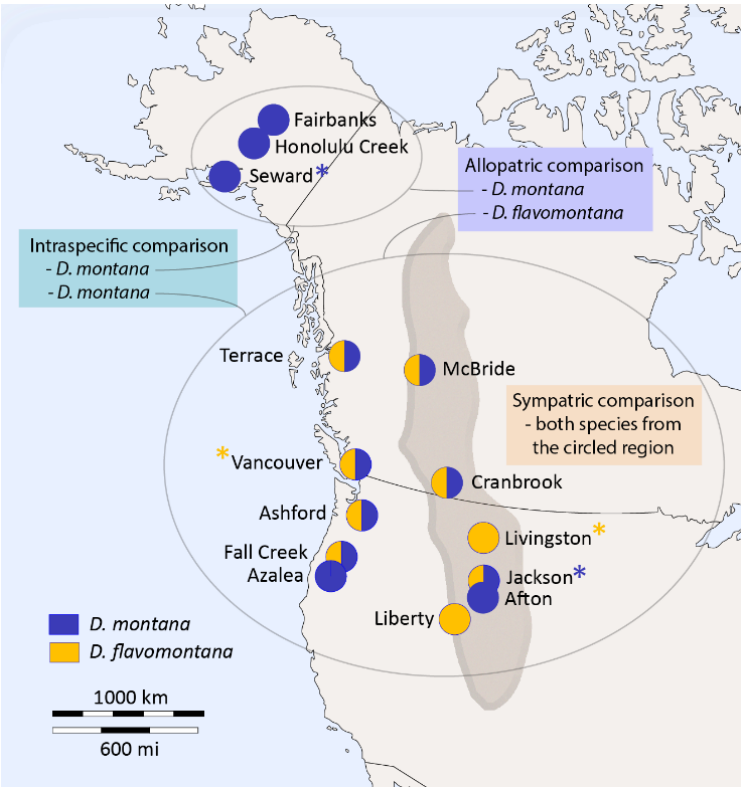

Figure 1. Sampling sites of sympatric (or parapatric) and allopatric *D. montana* and *D. flavomontana* populations in North America. Pie charts indicate the sampling sites for one or both species. PacBio data was obtained from the pools of females from one isofemale strain originating from the sample sites indicated with asterisks. Illumina data was obtained for single wild-caught females for all sites with and without asterisks. Detailed information on sequenced samples is given in Table S1.

Results and Discussion

We generated PacBio (Pacific Biosciences) sequencing data for females from two *D. montana* and two *D. flavomontana* isofemale strains originating from allopatric and sympatric populations (Fig. 1; Table S1). We also generated Illumina re-sequencing data for 12 *D. montana* and 9 *D. flavomontana* wild-caught females (one female per population per species). These data enabled us to generate contiguous high-quality genome assemblies for both species and accurately identify alternatively fixed inversions between the species, as well as to examine species' evolutionary history and the role of inversions and introgression therein. In species comparisons, *D. montana* and *D. flavomontana* samples from the Rocky Mountains and western coast are referred as "sympatry", and the comparisons between *D. montana* from Alaska and *D. flavomontana* from the mountains and the coast as "allopatry" (Fig. 1; Table S1).

Construction and annotation of species genomes

Two contiguous genome assemblies for each species were generated using the PacBio data of two *D. montana* and *D. flavomontana* isofemale strains and the Illumina data for the respective founder females collected from the wild (Table S1, Table S2). The assembled genomes had a total length of 181-194 Mb (Table 1), which resemble those of previously assembled *D. montana*, *D. flavomontana* and several other *Drosophila* species (128-198 Mb) (Miller et al. 2018; Parker et al. 2018; Yusuf et al. 2022). A small proportion of each assembly (0-18 contigs; span = 0.0-9.9 Mb) was excluded as contaminant sequences, mainly bacteria, based on the coverage, GC% and taxonomic annotation of contigs (Fig. S1-S4). From the 3285 BUSCO groups, 96.9-98.0% were complete single-copy BUSCOs, while 0.4-0.5% could not be identified (Table 1). The BUSCO values were similar to the ones in other *Drosophila* assemblies (Miller et al. 2018). Repetitive sequences comprised 25.5-29.9% of our assemblies (Table

1), which is close to the repeat content reported for other *Drosophila* species (e.g. 26.5% in *D. virilis*, 28.6% in *D. melanogaster*, 22.9% in *D. mojavensis*, and 19.9% in *D. elegans*; NCBI Annotation Report). Finally, we annotated 15,696-16,047 genes in each assembly, which falls within the range of 14,699-17,730 identified genes for other *Drosophila* species (e.g. (Yang et al. 2018)). Our combination of long- and short-reads resulted in more contiguous and complete assemblies for both species compared to the previously published *D. montana* and *D. flavomontana* genomes generated only from short-read data (Parker et al. 2018; Yusuf et al. 2022). For example, the previous *D. montana* genome had an N50 of 41 kb compared to the N50 values of 1.3-11.0 Mb in our assemblies (Table 1).

We built a chromosome-level reference genome for *D. montana* by scaffolding with *Drosophila lummei* genome, and for *D. flavomontana* by first scaffolding one assembly with the other (within species) and then with the *Drosophila lummei* genome (details in Methods). For both chromosome-level genomes, the total genome size, BUSCO values and the number of repeats and genes slightly decreased compared to the original, non-scaffolded assemblies (Table 1). Given the longer genome and higher BUSCO values of the *D. montana* chromosome-level reference genome, subsequent analyses were performed using the *D. montana* genome as a reference by default. However, to quantify the effect of reference bias we repeated the demographic inference using *D. flavomontana* as a reference.

Table 1. Genome contiguity, completeness and annotation of assemblies. N50 = half of the genome is in contigs larger than or equal to the N50 contig size. N50 count = half of the genome consists of the number indicated in N50 count.

		D. montana Seward, USA monSE13F37	*D. montana* Jackson, USA monJX13F48	*D. flavomontana* Livingston, USA flaMT13F11	*D. flavomontana* Vancouver, Canada flaVAN14F20	*D. montana* chromosome-level reference genome	*D. flavomontana* chromosome-level reference genome
Genome contiguity							
	Genome size (Mb)	184.3	181.0	192.6	193.5	145.5	142.3
	Total contigs	324	796	376	296	6	6
	Longest contig (Mb)	29.1	15.2	29.0	26.8	32.5	30.7
	N50 (Mb)	11.0	1.3	9.8	7.8	26.5	27.2
	N50 count	5	20	6	6	3	3
Genome completeness							
	Total complete BUSCOs (%; n: 3285)	98.1	98.5	97.5	97.3	91.9	91.5
	Single copy BUSCOs (%)	97.6	98.0	97.1	96.9	91.7	91.2
	Duplicated BUSCOs (%)	0.5	0.5	0.4	0.4	0.2	0.3
Genome annotation							
Repeat elements	**GC level (%)**	40.2	40.2	40.2	40.1	40.3	40.3
	Masked repeats (%)	26.6	25.5	29.9	28.2	16.8	15.1
Gene annotation	**Genes (N)**	15,696	15,819	15,940	16,047	15,446	14,901
	Mean gene length (bp)	1,640	1,637	1,568	1,564	1,571	1,557
	Total complete BUSCOs (%; n: 3285)	94.2	94.7	92.5	92.9	88.5	87.3
	Single copy BUSCOs (%)	84.4	84.5	84.1	84.5	79.9	79.3
	Duplicated BUSCOs (%)	9.8	10.2	8.4	8.4	8.8	8.0

Genetic differentiation of *D. montana* and *D. flavomontana* populations from climatically diverse regions with different species compositions

We visualised the variation in the Illumina re-sequence data of wild-caught *D. montana* and *D. flavomontana* females from different parts of North America with different species abundancies (Table S1, S2) to trace the species' evolutionary history. We first summarised genetic differentiation of the samples in a principal component analysis (PCA) using 9,064,171 filtered SNPs (from coding, intronic and intergenic regions). The first principal component (PC1) explained 50% of the total genetic variance and clearly separated *D. montana* and *D. flavomontana* samples from each other (Fig. 2A, Table S4). PC2 explained 4% of the total variance and captured mainly variation in *D. montana*, while variation in *D. flavomontana* was lower (Fig. 2A; Table S4). PC2 separated Alaskan (allopatric) *D. montana* populations (Honolulu Creek, Seward, Fairbanks) from the other *D. montana* populations, but also showed some variation among non-Alaskan populations (Fig. 2A).

Next, we explored climatic patterns of fly sampling sites to determine the extent to which climatic conditions may have affected the genetic differentiation of the samples. We performed a PCA on 19 bioclimatic variables of each fly sampling site (Table S5, Table S6) to reduce correlations between the variables and summarized climatic patterns prevailing in the sites. This PCA revealed three principal

components (PCs) with eigenvalues >1, of which the first two PCs explained 80% of the climatic variation (Fig. 2B; Table S7). The first PC clearly separated inland and coastal populations and suggested that populations from the mountainous inland experience cold winters and high seasonal temperature variation, while coastal populations experience milder temperatures and high precipitation throughout the year (Fig. 2B; Table S8). The second PC separated populations based on latitude and summer temperatures and distinguished Alaskan populations (Honolulu Creek, Seward, Fairbanks) from the other populations (Fig. 2B; Table S8).

Together these results show that *D. montana* and *D. flavomontana* populations are genetically diverged regardless of their climatic origin and species coexistence. Genetic differentiation was greater among *D. montana* populations than among *D. flavomontana* populations, which is likely due to *D. montana*'s larger distribution area and the fact that *D. flavomontana* has spread across North America more recently than *D. montana* (Hoikkala and Poikela 2022). Finally, the genetic differentiation between allopatric (from Alaska) and sympatric (from the Rocky Mountains and the western coast) *D. montana* populations likely reflects a demographic history of intraspecific divergence, local adaptation to climatic conditions, or both.

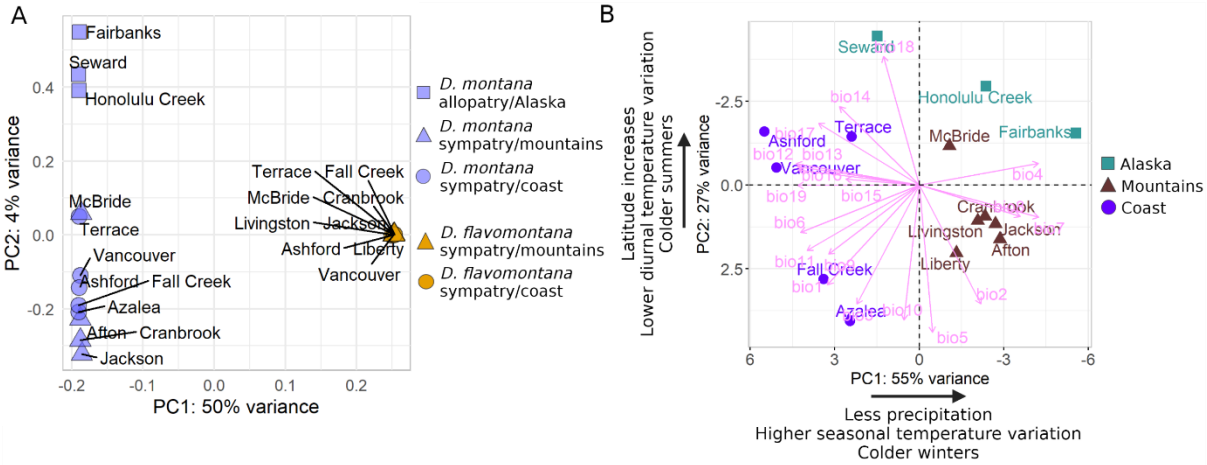

Figure 2. A principal component analysis (PCA) (A) on whole-genome SNP data of *D. montana* (*D. mon*) and *D. flavomontana* (*D. fla*) samples originating from different sites of North America and (B) on 19 bioclimatic variables (detailed explanations in Table S5) of each fly sampling site.

D. montana and *D. flavomontana* chromosomes differ by several large inversions

We combined long- and short-read genomic data to characterize inversion breakpoints in *D. montana* and *D. flavomontana*. We identified several large (>0.5kb) inversions that were alternatively fixed between North American *D. montana* or *D. flavomontana* samples (Fig. 3; Table S9). The X chromosome contained three partly overlapping inversions, two of which were fixed in *D. montana* (7.2Mb and 14.2Mb) and one in *D. flavomontana* (3.2Mb) (Fig. 3; Table S9). The left arm of the 2nd chromosome (2L) contained one inversion fixed in *D. montana* (3.9Mb), and chromosomes 4 and 5 each contained one inversion fixed in *D. flavomontana* (13.8Mb and 9.2Mb, respectively) (Fig. 3; Table S9). The sizes of *D. montana* and *D. flavomontana* inversions were obtained from the reference genomes of each species (Table S9). All inversions were homozygous in the studied Illumina samples (Table S9), except the 2L inversion, which was heterozygous in all *D. montana* samples. The right arm of the 2nd chromosome (2R) and the 3rd chromosome were not found to contain any inversions (Fig. 3). Based on the old polytene chromosome studies, where rearrangements were observed from salivary gland chromosomes using microscopy, the three alternatively fixed inversions between *D. montana* and *D. flavomontana* on the X chromosome were named E, F and G (Stone et al. 1960). These inversions could not be distinguished in more detail, and in contrast to our results, Stone et al. (1960) suggest that all of them are fixed in *D. flavomontana*. The inversions on the 4th and 5th chromosome have been named J

and E, respectively, in karyotype studies, but the 2L inversion could not be assigned to its previous name (Stone et al. 1960)

The average size of the inversions fixed in *D. montana* was 8.4Mb and those in *D. flavomontana* 9.4Mb. The X chromosome contained a higher number of inversions between these species than the autosomes (Fig. 3, Table S9). The average size of the reported inversions is 8.4 Mb both in animals and plants (Wellenreuther and Bernatchez 2018). Inversion frequencies are known to vary greatly between closely related *Drosophila* species: for example, *D. virilis* has no inversions while both its close relatives *D. americana* and *D. novamexicana* and more distant relatives including *D. montana* and *D. flavomontana* have several (Stone et al. 1960). It is not clear whether large inversions are common because of an observational bias, or because they suppress recombination between a larger set of locally adapted genes relative to shorter inversions and are thus under stronger positive selection (Wellenreuther et al. 2019). Our finding of a larger number of inversions on the X is consistent with theory showing that the fixation probability of X chromosomal inversions is higher than that of autosomal inversions, because selection can more effectively favour beneficial and purify deleterious recessive X-linked alleles than autosomal ones (Charlesworth et al. 1987; Vicoso and Charlesworth 2006; Charlesworth et al. 2018; Connallon et al. 2018).

The polytene chromosomes studies by Stone et al. (1960) and Throckmorton (1982) suggest that *D. montana* and *D. flavomontana* carry additional inversions that were not identified in this study. In particular, *D. flavomontana* may harbour one fixed inversion of unknown size on the 3rd chromosome (inversion E; (Stone et al. 1960)), which we might have missed due to the higher fragmentation of this chromosome compared to the other chromosome contigs (Table S3). Given our limited sample size and the explicit focus on fixed inversion differences, polymorphic inversions previously found in these species (Stone et al. 1960), which may be associated with local adaptation or other evolutionary processes within species (Fang et al. 2012; Kapun et al. 2016; Wallberg et al. 2017), were not identified here.

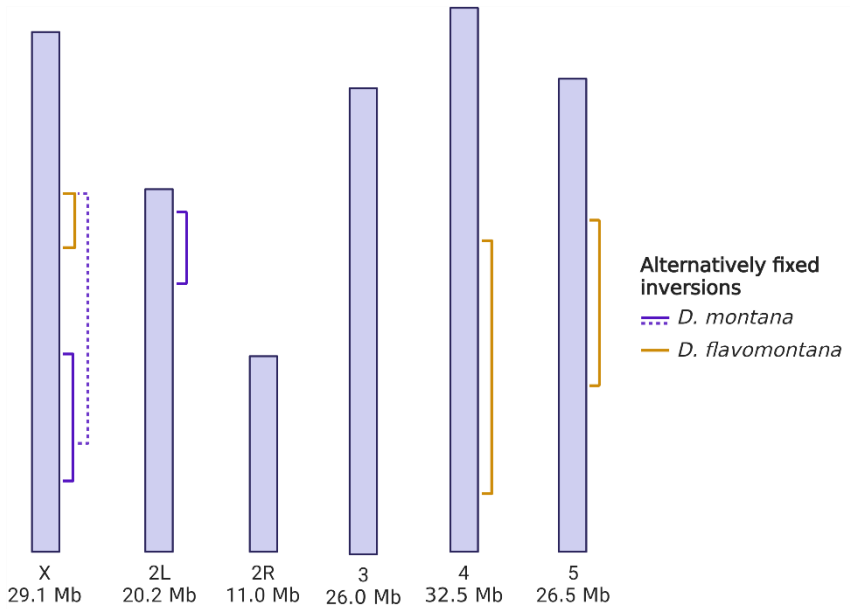

Figure 3. Chromosomes and large alternatively fixed inversions of *D. montana* (blue solid and dashed lines) and *D. flavomontana* (orange solid lines) (Table S9). The inversions are illustrated against *D. montana* chromosome-level genome coordinates and the numbers below each chromosome refer to its length in the assembly. Chromosome 2 has left (2L) and right (2R) arms that are separated by a submetacentric centromere.

250 Genetic divergence between *D. montana* and *D. flavomontana* is greater inside than outside inversions

251 We analysed the mean genetic divergence (d_{XY}) to test whether inversions have reduced recombination
252 and introgression between *D. montana* and *D. flavomontana*, and if so, whether it is ancient or recent.
253 In the latter case, d_{XY} should be lower in sympatry compared to allopatry (Harrison and Larson 2014).
254 We estimated d_{XY} separately for coding, intronic and intergenic sequences and inverted and colinear
255 regions of the genome. These analyses were carried out for allopatric and sympatric comparisons of
256 the species as well as for intraspecific comparisons of *D. montana* populations (allopatric and sympatric
257 *D. montana*). Given the potentially different evolutionary history of the X chromosome and autosomes
258 (Vicoso and Charlesworth 2006; Charlesworth et al. 2018), analyses for the X (both colinear and
259 inverted regions) were performed separately.

260 Mean d_{XY} values (between *D. montana* and *D. flavomontana*, and between the two *D. montana*
261 populations) were remarkably similar for intergenic and intronic sequences but much lower in coding
262 sequences (Fig. 4), as expected given the stronger selective constraint on coding sequence (Halligan
263 and Keightley 2006).

264 d_{XY} was slightly, but consistently lower in sympatric compared to allopatric comparisons of the species
265 across all chromosomal regions (Fig. 4; Table S10). Moreover, genetic divergence at non-coding (i.e.
266 intergenic and intronic) sequences was consistently higher in inverted compared to colinear regions in
267 allopatric and sympatric comparisons (Fig. 4; Table S10). We also found increased d_{XY} at coding sites for
268 inversions on the 4th and the X chromosome compared to colinear regions both in allopatry and
269 sympatry (Fig. 4; Table S10). In contrast, the 2L inversion had lower d_{XY} at coding sites compared to the
270 colinear regions in sympatry. The comparisons of d_{XY} at inverted and colinear regions were less clear
271 cut within *D. montana* (Fig. 4; Table S10). d_{XY} was significantly higher for the regions containing the 4th
272 and the X inversions (intergenic, intronic and coding sequences) and significantly lower in the regions
273 containing the 2L inversion (intergenic, intronic and coding sequences) compared to the colinear
274 regions (Fig. 4; Table S10). Plotting d_{XY} in sliding windows showed an increase in genetic divergence,
275 especially around the inversion breakpoints and for X chromosomal inversions, for interspecific, but not
276 intraspecific comparisons (Fig. 5).

277 Overall, our finding of consistently higher genetic divergence of the non-coding sequences inside
278 compared to outside of inversions supports the idea that inversions suppress gene exchange and
279 facilitate the accumulation of genetic differences (Fig. 4; (Navarro and Barton 2003; Kirkpatrick and
280 Barton 2006)). We also find that genetic divergence was highest around inversion breakpoints and in
281 the series of overlapping inversions on the X (Fig. 5), where recombination is most suppressed
282 (Hoffmann and Rieseberg 2008). Similar signatures of elevated genetic divergence between closely
283 related species inside and around inversion breakpoints have been detected in other *Drosophila* species
284 pairs (Noor et al. 2007; Kulathinal et al. 2009; Lohse et al. 2015), *Helianthus* sunflowers (Barb et al.
285 2014), *Sorex* shrews (Basset et al. 2006), and *Anopheles* mosquito (Michel et al. 2006). Furthermore,
286 our finding of lower genetic divergence in sympatry compared to allopatry (Fig. 4) is consistent with
287 low levels of recent introgression in sympatry (Noor and Bennett 2009).

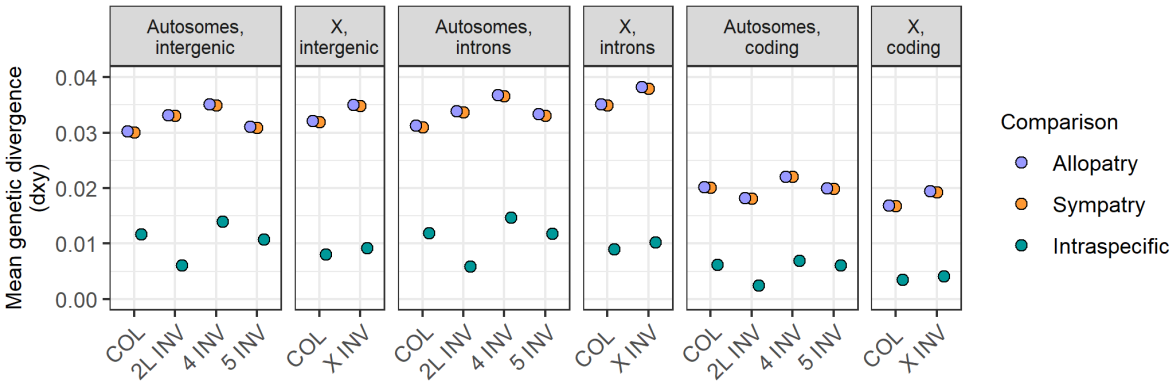

Figure 4. Mean genetic divergence (measured as d_{XY}) at intergenic, intronic and coding sequences, for autosomal and X chromosomal colinear (COL, background) and inverted (INV) chromosomal regions. Divergence is shown for allopatric and sympatric comparisons of *D. montana* and *D. flavomontana* and for intraspecific comparisons of *D. montana.* P-values are shown in Table S10.

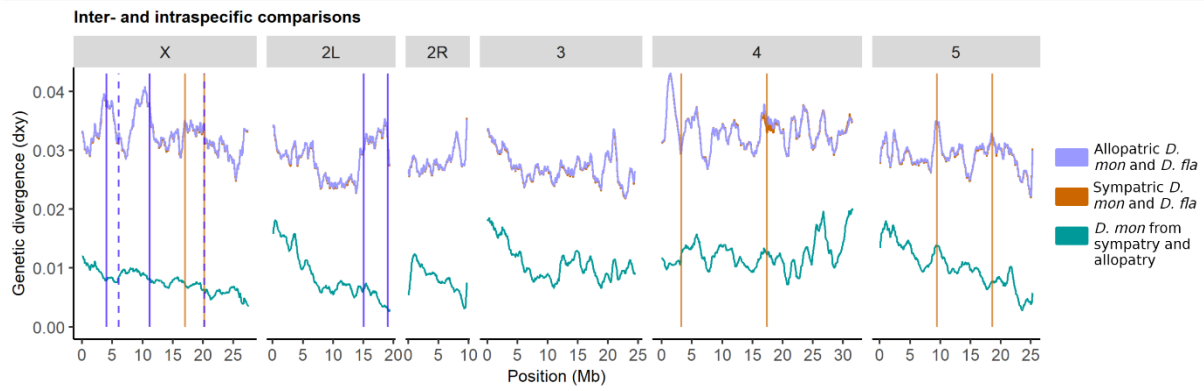

Figure 5. Genetic divergence across the genome (coding, intronic and intergenic regions) in sliding windows for allopatric and sympatric comparisons of *D. montana* and *D. flavomontana* (interspecific), and for *D. montana* originating from allopatry and sympatry (intraspecific). Inversion breakpoints of *D. montana* (blue) and *D. flavomontana* (orange) are marked with vertical lines (solid and dashed lines represent breakpoints of different inversions; see Fig. 3).

Hierarchical model comparison suggests species have diverged with a very low levels of post-divergence gene flow from *D. montana* to *D. flavomontana*

We used an analytic likelihood method to fit a series of demographic models of species divergence with and without long-term post-divergence gene flow, i.e. isolation with migration (IM) and strict divergence (DIV) models (Fig. 7) to the data summarised in terms of the bSFS (see Methods). The evolutionary history of the X chromosome (Vicoso and Charlesworth 2006; Charlesworth et al. 2018) and inversions may differ from other regions and these genomic partitions were therefore analysed separately from colinear, autosomal regions. Thus, our initial model comparison was based on only intergenic sequences of colinear autosomal regions (repetitive regions were excluded). We performed separate analyses for sympatric and allopatric comparisons of *D. montana* and *D. flavomontana* and for intraspecific comparison of *D. montana.* We carried out this initial model comparison twice, using both *D. montana* and *D. flavomontana* as a reference genome, to evaluate the potential effects of reference bias. Parameter estimates and support values (lnCL) under all demographic models are shown in Table 2 for 64 bp blocks and using *D. montana* as a reference (analogous analyses for all four combinations of block length and reference genomes are given in Table S11).

For both allopatric and sympatric comparisons (and for three of the four combinations of reference genomes and block sizes used), the best-fitting demographic scenario was an IM model assuming introgression from *D. montana* into *D. flavomontana* (Table 2, S11). Our parametric bootstrap analyses

showed that the improvement in fit of this IM model compared to the DIV model was significant suggesting a low but genuine signal of introgression (Fig. S5, S6). The only exception was the analysis using *D. flavomontana* as a reference genome and shorter blocks (64bp). In this case, the DIV model could not be rejected (Fig. S5, S6). However, estimates for all parameters (T and the three N_e parameters) were extremely similar regardless of the model (DIV and IM), block size (64bp and 128bp) and reference genome (*D. montana* and *D. flavomontana*) used (Table S11). Given the overall support for post-divergence gene flow and inherent bias of methods such as gIMble to underestimate migration rates (M), we present the IM model as the best fitting/most plausible scenario throughout. Accordingly, the subsequent analyses were conducted assuming an IM model with migration from *D. montana* into *D. flavomontana* (Table 2). Yusuf et al. (2022) also recently found signatures of introgression between *D. montana* and *D. flavomontana* using a different approach, which gives further support for our introgression signal.

For the intraspecific comparison within *D. montana*, the DIV model could not be rejected in any analysis. When using 64bp blocks, DIV and IM models had equal support, irrespective of which species was used as a reference (Table 2, S11). Analyses based on longer blocks (128bp) estimated slightly higher support for an IM model assuming post-divergence gene flow from allopatric (Alaskan) *D. montana* to sympatric (coastal/mountain) *D. montana* (Table 2, S11). However, our parametric bootstrap analyses showed that the associated improvement in fit compared to the simpler DIV model was non-significant. Thus, the DIV model could not be rejected (Table S5, S6). It is possible that allopatric *D. montana* populations exchange genetic material with the closest sympatric *D. montana* populations (e.g. Terrace and McBride) but not with the more distant ones, and thus the genuine post-divergence gene flow signal was not detected. Consequently, the subsequent intraspecific analyses were conducted using the DIV model (Table 2).

Table 2. Support (measured as ΔlnCL) and parameter estimates for divergence time (T), migration rate (M) and effective population sizes (N_e) for studied populations and their common ancestral population under strict divergence (DIV, M=0) and isolation with migration (IM) models with both gene flow directions. The model comparison is based on the *D. montana* reference genome and block size 64 bp, and was performed for intergenic autosomal colinear regions to minimize the effects of selection. Grey shading indicates the best-fit model for each comparison.

Comparison	Model	*D. mon* Ne	*D. fla* Ne	Ancestral Ne	T	M	lnCL	ΔlnCL
Allopatric comparison	DIV	714914	400196	1460808	2405724	-	-43059297	12929
(*D. mon* vs *D. fla*)	IM *D. mon --> D. fla*	728215	386120	1395634	2573631	1.13E-08	-43046368	0
	IM *D. fla --> D. mon*	714135	400661	1453429	2426511	1.27E-09	-43059034	12666
Sympatric comparison	DIV	746171	397288	1453485	2370833	-	-129149797	48447
(*D. mon* vs *D. fla*)	IM *D. mon --> D. fla*	762494	380755	1378191	2564214	1.34E-08	-129101350	0
	IM *D. fla --> D. mon*	744781	398093	1441519	2405381	2.21E-09	-129147830	46480
	Model	***D. mon allop* Ne**	***D. mon symp* Ne**	**Ancestral Ne**	**T**	**M**	**lnCL**	**ΔlnCL**
Intraspecific comparison	DIV	1150743	1688437	876904	227573	-	-38019871	0
(*D. mon* vs *D. mon*)	IM *D. mon symp. --> D. mon allop.*	1150745	1688438	876904	227573	3.38E-16	-38019871	0
	IM *D. mon allop. --> D. mon symp.*	1150695	1687674	876901	227611	1.65E-09	-38019871	0

Species-specific inversions were fixed earlier or around the species' split and introgression was lower inside compared to outside of inversions and in allopatry compared to sympatry

We used the best-fit isolation with migration (IM) model (Table 2) to examine the speciation history of *D. montana* and *D. flavomontana* and test the potential role of inversions and introgression in their speciation process. As before, the analysis was limited to intergenic regions to minimize the effects of selection, and separate analyses were carried out for the X chromosome and autosomes and for inverted and colinear regions. To estimate the timing of potential recent introgression, we also analysed the split time for *D. montana* living in contact (sympatry) or in isolation (allopatry) with *D. flavomontana* using the simpler strict divergence (DIV) model (intraspecific comparison; Table 2).

Taking the estimates for the colinear autosomal background as face value, *D. montana* and *D. flavomontana* have diverged ca 3.4 Mya (Fig. 6A, 6C). The divergence time estimates of the inversions

differ from each other, and the inversions on the 4th, 5th and the X chromosome predate the divergence time estimated for the colinear background (ca 3.6-4.0 Mya) (Fig. 6A, 6C; Table S12). In contrast, the 2L inversion has fixed after the onset of species divergence (ca 3.1 Mya) (Fig. 6A, 6C; Table S12). For all chromosome partitions, genetic diversity (Pi) and effective population size (N_e) of *D. montana* were approximately two times as large as those of *D. flavomontana* (Fig. S7, S8). *D. montana* populations living in contact (sympatry) and in isolation (allopatry) with *D. flavomontana* have diverged much more recently than *D. montana* and *D. flavomontana*, approximately 350 000 years ago (Fig. 6C).

Introgression from *D. montana* to *D. flavomontana* was lower inside than outside inversions both for the autosomes and for the X chromosome (Fig. 6B; Table S13), which is in accordance with the finding that genetic divergence of non-coding (intergenic and intronic) sequences was consistently higher inside than outside of inversions (Fig. 4; Table S10). Moreover, the migration rate estimates were significantly higher in sympatry compared to allopatry (Fig. 6B; Table S14), which agrees with the slightly, but consistently lower genetic divergence in sympatric compared to allopatric comparisons of the species (Fig. 4; Table S10).

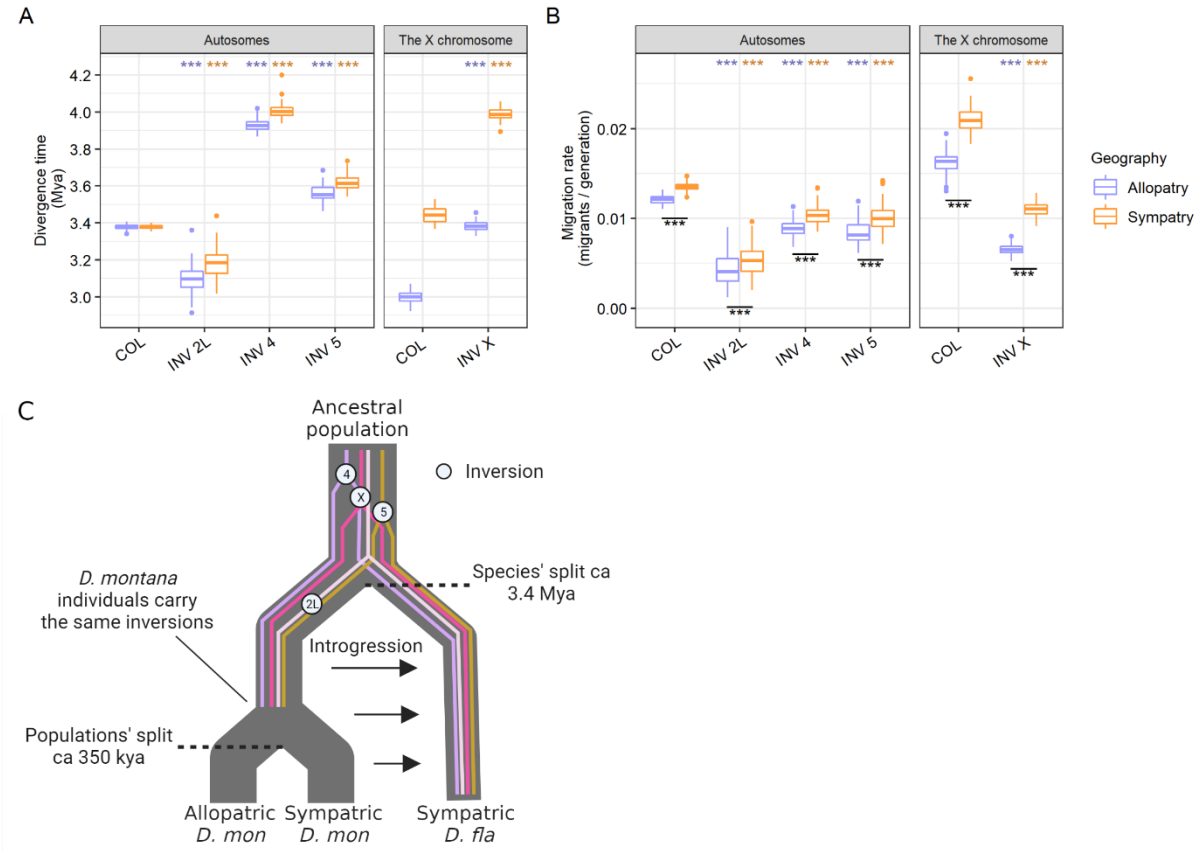

Figure 6. (A) The split times and (B) migration rate for different chromosomal regions and for *D. montana* and *D. flavomontana* originating from allopatric and sympatric populations. Confidence intervals were inferred using simulations under the best-fit IM model (simulated 100 times). Significance levels were obtained from generalized linear models (*** $P < 0.001$), where i) colinear region (COL, background) was compared to inverted (INV) regions separately for autosomes and the X chromosome and for allopatric and sympatric comparisons (significances above boxplots), and where ii) differences in migration rate between allopatric and sympatric populations were compared within each chromosomal region (significances below boxplots). Whiskers represent ±1.5×IQR. (C) Illustration of the likely evolutionary history of *D. montana* and *D. flavomontana* (split times are rough mean estimates across allopatric and sympatric comparisons).

Taken together, our analyses suggest that *D. montana* and *D. flavomontana* diverged ca 3-4 Mya (depending on the analysed regions), which is close to the recent estimate of 3.8 Mya based on 1336 single-copy orthologs and 100 randomly sampled small introns (Yusuf et al. 2022). All fixed inversions

in *D. montana* and *D. flavomontana*, except the inversion on 2L, predate the species split, and so must have existed already in the common ancestral population. According to Noor and Bennett (2009) and Fuller et al. (2018), the elevated genetic divergence observed within inversions predating species divergence is likely a consequence of reduced recombination and gene flow between locally adapted populations in the common ancestor rather than from a reduction in post-divergence gene flow or ongoing introgression. This is further supported by the fact that the estimated long-term rate of migration from *D. montana* to *D. flavomontana* was extremely small and several orders of magnitude lower than e.g. a similar estimate for *Drosophila mojavensis* and *Drosophila arizonae* (Lohse et al. 2015). *D. mojavensis* and *D. arizonae* have approximately one migrant per generation, while our estimate for *D. montana* and *D. flavomontana* is roughly 1 migrant in 80 generations. Thus, even the total probability of a lineage sampled in *D. flavomontana* to trace back to *D. montana* via migration (1-e^(-T M)) is only 3.4%.

Fuller et al. (2018) have recently proposed that ancestrally segregating inversions may act as slowly progressing drivers of speciation, by accumulating positively selected genetic differences conferring early ecological divergence, prezygotic barriers and an incidental build-up of genetic incompatibilities. Colinear regions, on the other hand, can keep mixing until the formation of strong reproductive isolation. For example, selection against introgressed ancestry in the new genetic background may generate reinforcement via prezygotic barriers to prevent maladaptive hybridization, and eventually complete the speciation process (Servedio and Noor 2003). Our results support this idea, and in fact, we have recently shown with experimental approach that introgression from *D. montana* to *D. flavomontana* across the X chromosome is prevented by a dominant incompatibility locus residing within the overlapping X chromosomal inversions (Poikela et al. 2022). However, we cannot verify whether the incompatibility allele on the X has evolved before or around the species' split, or afterwards (post-speciation event), and whether the lower migration rate inside compared to outside of inversions is a consequence of direct selection against introgression or simply the reduced recombination between alternate rearrangements. In contrast to the other inversions, the 2L inversion has fixed after the onset of species' divergence and shows lower levels of introgression than the other inversions, which may indicate strong selection against introgression. This could potentially imply causality between the fixation of the 2L inversion and the completion of speciation. With a similar approach, Lohse et al. (2015) showed that introgression between *D. mojavensis* and *D. arizonae* had ceased around the time when multiple overlapping inversions had fixed around the species split.

The low levels of introgression between *D. montana* and *D. flavomontana* observed here agree well with our previous evidence for strong pre- and postzygotic barriers between the species (Poikela et al. 2019). Also, species' differences in the usage of host trees and their ability to tolerate cold, accompanied with altitudinal and latitudinal variation in their distribution (Throckmorton 1982; Poikela et al. 2021), might have contributed to species' ecological isolation and reduced their encounters in nature. Intriguingly, we found higher levels of introgression in sympatry compared to allopatry, which suggests at least some gene flow from *D. montana* to *D. flavomontana* over the past ~350 000 years, i.e. after the allopatric (Alaskan) *D. montana* population diverged from *D. montana* coexisting with *D. flavomontana*. This is consistent with our previous finding that *D. flavomontana* has developed stronger prezygotic barriers against *D. montana* in sympatry compared to allopatry, presumably as a result of reinforcement (Poikela et al. 2019). Even low levels of introgression can facilitate strengthening of prezygotic barriers to prevent maladaptive hybridization between species (Servedio and Noor 2003; Cruickshank and Hahn 2014).

Even though many species pairs differ from each other by multiple inversions, the majority of inversion differences must have arisen after speciation (Faria and Navarro 2010). Performing pairwise comparisons for younger and older species would offer a more holistic view of the role of inversions in speciation events. In our case, characterizing inversions and investigating divergence times and introgression across all species of the *montana* phylad of the *virilis* group (*D. montana*, *D. flavomontana*, *D. borealis* and *D. lacicola*) (Hoikkala and Poikela 2022) could provide valuable additional information.

In general, investigating millions of years old events by fitting necessarily drastically simplified scenarios of reality involve uncertainties. Experimental approaches, potentially with the help of CRISPR/Cas9 gene editing technique, could allow the creation of artificial inversions or reversion of existing ones, and direct tests of the role of inversions in speciation (Faria and Navarro 2010; Faria et al. 2018; Hopkins et al. 2020; White et al. 2020).

Conclusions

It has proven extremely difficult to test if and how inversions facilitate speciation, and empirical evidence on the role of inversions in speciation is largely lacking (Faria and Navarro 2010; Fuller et al. 2019). We explored these questions in two sister species of the *D. virilis* group, *D. montana* and *D. flavomontana*. Our main goals were (1) to characterize alternatively fixed chromosomal inversions of *D. montana* and *D. flavomontana*, (2) to investigate the age of the inversions, and (3) to identify whether the inversions have restricted recombination between *D. montana* and *D. flavomontana*, and either protected existing genetic incompatibilities in secondary contact, or have facilitated the accumulation of incompatibilities in the presence of gene flow.

Taking advantage of long- and short-read genome sequencing technologies, we were able to generate the high-quality contiguous reference assemblies for *D. montana* and *D. flavomontana*. These genomes enabled us to accurately characterize inversions that are alternatively fixed between these sister species across their distribution area in North America. We were able to assign the majority of these to inversions that were described for the species already in the 1950s and 1960s based on polytene chromosome studies (Stone et al. 1960). Our analyses show clearly that the inversions on the 2L, 4th, 5th and the X chromosome arose either before or at the onset of species divergence. Thus, the elevated genetic divergence inside compared to outside of inversions results most likely from restricted recombination and gene flow between locally adapted populations of the ancestral form. Accordingly, our results support the idea that ancestrally polymorphic inversions can drive the speciation process by aiding the accumulation of genetic incompatibilities (Fuller et al. 2018), while colinear regions keep exchanging genetic material until strong reproductive isolation has formed. This is also supported by our recent finding that the X chromosomal inversions contain a strong incompatibility locus that effectively restricts introgression between *D. montana* and *D. flavomontana* in the first few backcross generations (Poikela et al. 2022).

Overall, our study suggests that inversions may indeed be early triggers in the speciation process and highlights the value of interpreting the evolutionary effects of inversions through the lens of demographic models. However, in doing so, we have ignored much of the mechanistic and selective detail of inversion evolution. Regions with repetitive sequences, such as transposable elements, tRNAs, ribosomal genes or segmental duplications, are prone to breakage and are often the initial source of an inversion (Kapun and Flatt 2018). Investigating repetitive sequences or small structural variations around the inversion breakpoints would increase our understanding on how the inversions originated in the first place. Moreover, inversions are not static through their lifetime, but evolve in response to changes in selection, genetic drift, new mutations and gene flux (occurring via double cross-overs and gene conversion), as well as by interactions with colinear genome or with other inversions (Faria et al. 2018). Given the many, sometimes entangled processes affecting the origin and the fixation of inversions, models that can extract information about both demography and the selective forces acting on inversions in the early stages of speciation are the next obvious step in understanding how inversions facilitate the origin of species (Faria et al. 2018).

478 ## Materials and Methods

479 ### Sample collections and maintenance

480 *D. montana* and *D. flavomontana* females were collected from several sites in the Rocky Mountains and
481 the western coast of North America, and Alaska between 2013 and 2015 (Fig. 1; Table S1). Sites in the
482 Rocky Mountains and the western coast of North America are either inhabited by both species
483 (sympatric sites: Jackson, Cranbrook, McBride, Terrace, Vancouver, Ashford, Fall Creek), or by one of
484 the species with nearby sites inhabited by both species (parapatric sites: Liberty, Afton, Livingston,
485 Azalea) (Fig. 1, Table S1). *D. montana* also has stable populations in high latitudes in Alaska, where *D.*
486 *flavomontana* does not exist. We refer to the comparisons between *D. montana* and *D. flavomontana*
487 from the Rocky Mountains and from the western coast as "sympatry", and those between *D. montana*
488 from Alaska and *D. flavomontana* from the Rocky Mountains or the western coast as "allopatry" (Fig.
489 1).

490 The newly collected females were brought to the fly laboratory, with a constant light, 19±1 ˚C and ~60%
491 humidity, in the University of Jyväskylä, Finland. Females that had mated with one or several males in
492 nature were allowed to lay eggs in malt vials for several days, after which they were stored in 70% EtOH
493 at -20 ˚C. The emerged F_1 progeny of each female were kept together to produce the next generation
494 and to establish isofemale strains. After that also the F_1 females were stored in 70% EtOH at -20 ˚C.

495 ### DNA extractions and sequencing

496 We performed PacBio long-read sequencing and generated four genome assemblies from two *D.*
497 *montana* and two *D. flavomontana* isofemale strains that had been kept in the fly laboratory since their
498 establishment (Fig. 1; Table S1). DNA of the Seward *D. montana* and both *D. flavomontana* samples
499 were extracted from a pool of 60 three days old females per isofemale strain using
500 cetyltrimethylammonium bromide (CTAB) solution with RNAse treatment, Phenol-Chloroform-Isoamyl
501 alcohol (25:24:1) and Chloroform-Isoamyl alcohol (24:1) washing steps, and ethanol precipitation at the
502 University of Jyväskylä, Finland. DNA of the Jackson *D. montana* sample was extracted with the "DNA
503 Extraction SOP For Animal Tissue" protocol and purified with Ampure beads at BGI (Beijing Genomics
504 Institute). Quality-checked DNA extractions of the Seward *D. montana* sample and both *D.*
505 *flavomontana* samples were used to generate >15 kb PacBio libraries, which were all sequenced on two
506 SMRT cells within a PacBio Sequel system (Pacific Biosciences, United States) at the Norwegian
507 Sequencing Centre. DNA of the Jackson *D. montana* sample was used to generate >20 kb PacBio
508 libraries and was sequenced on one SMRT cell using the PacBio Sequel system at BGI. Average PacBio
509 raw read coverage was 27-35X per sample, except for the Jackson *D. montana* sample which was
510 sequenced at 63X coverage. Detailed information on the PacBio raw reads of each sample is provided
511 in Table S2.

512 We generated Illumina re-sequencing data for 12 *D. montana* and 9 *D. flavomontana* single wild-caught
513 females or their F_1 daughters from several locations in North America (Fig. 1; Table S1). DNA extractions
514 were carried out at the University of Jyväskylä, Finland, using a CTAB method as described above.
515 Quality-checked DNA was used to produce an Illumina library for each sample in three batches. First,
516 Nextera libraries were used to generate 150 bp paired-end (PE) reads on two lanes using HiSeq4000
517 Illumina instrument by Edinburgh Genomics. Second, one Truseq library was used to generate 150 bp
518 PE reads on one lane of a HiSeq4000 Illumina instrument at the Norwegian Sequencing Centre. Third,
519 Truseq libraries were used to generate 150 bp PE reads on one lane of a HiSeq X-Ten Illumina
520 instrument at BGI. We generated on average 46-95X coverage per sample, except for the *D. montana*
521 sample from Seward, which was sequenced to 371X coverage. Detailed information on Illumina raw
522 reads is provided in Table S2.

523

524 Genome assemblies

525 We generated initial *de novo* assemblies for each PacBio dataset and the respective Illumina reads using
526 the wtdbg2 pipeline v2.5 (RedBean; Ruan & Li, 2020) and MaSuRCA hybrid assembler v3.3.9 (Zimin et
527 al., 2017). To improve assembly contiguity, we used quickmerge for both assemblies of each sample
528 (Chakraborty et al. 2016). The initial assembly statistics are given in Table S15. We polished the resulting
529 assemblies with the respective Illumina reads using Pilon v1.23 (Walker et al. 2014) and removed
530 uncollapsed heterozygous regions using purge_dups (Guan et al. 2020).

531 We identified genomic contaminants in the assemblies with BlobTools v1.1 (Laetsch and Blaxter 2017).
532 PacBio and Illumina reads were first mapped back to each assembly with minimap2 (Li, 2018) and BWA
533 mem (Burrows-Wheeler Aligner) v0.7.17 (Li & Durbin, 2009), respectively. Contigs in the assemblies
534 were then partitioned into taxonomic groups based on similarity search against the NCBI nucleotide
535 database (BLASTn 2.9.0+; Camacho et al., 2009) and Uniref90 (Diamond v0.9.17; Buchfink, Xie, & Huson,
536 2015). Finally, contigs were visualized on a scatter plot and coloured by putative taxonomic groups (Fig.
537 S1-S5). Non-Diptera contigs were removed manually from the assemblies based on sequence GC
538 content, read coverage and taxonomy assignment. We estimated the completeness of the assemblies
539 with the BUSCO pipeline v5.1.2 using the Diptera database "diptera_odb10" (Seppey, Manni &
540 Zdobnov, 2019), which searches for the presence of 3285 conserved single copy Diptera orthologues.

541 We constructed chromosome-level reference genomes for both species by scaffolding contigs of the
542 original assemblies with a reference-genome -guided scaffolding tool RagTag v2.1.0 (Alonge et al.,
543 2019), which orients and orders the input contigs based on a reference using minimap2 (Li 2018). We
544 used default settings except for the increased grouping confidence score (-i) which was increased to
545 0.6. We performed two rounds of RagTag. We first scaffolded the Seward *D. montana* assembly with
546 the Jackson *D. montana* assembly (which did not improve the assembly due to higher fragmentation of
547 the latter). For the second round of RagTag, we used the *Drosophila lummei* genome, which was
548 constructed using PacBio and Illumina reads and assigned to chromosomes using the published
549 *Drosophila virilis* chromosome map (Schäfer et al. 2010) and *D. virilis* assembly dvir_r1.03_FB2015_02
550 obtained from Flybase (Poikela et al. in prep.). Respectively, we scaffolded the Livingston *D.*
551 *flavomontana* assembly with the Vancouver *D. flavomontana* assembly and then with *D. lummei*. In *D.*
552 *montana* and *D. flavomontana*, chromosome 2 has right (2R) and left (2L) arms, separated by a
553 (sub)metacentric centromere, whereas in other *virilis* group species the centromere is located near one
554 end of the chromosome 2 (Stone et al. 1960). Therefore, scaffolding of chromosomes 2L and 2R was
555 not feasible with the *D. lummei* genome.

556 For the *D. montana* chromosome-level reference genome, the X chromosomes (29.1Mb), 2L (20.2Mb)
557 and 2R (11.0Mb) could not be further scaffolded and were kept as they are, while the lengths of
558 chromosomes 3, 4 and 5 were increased substantially by scaffolding. The longest contig of chromosome
559 3 increased from 5.8Mb to 26.0Mb (constructed from 37 contigs), that of chromosome 4 from 12.3Mb
560 to 32.5Mb (28 contigs), and that of chromosome 5 from 19.5Mb to 26.5Mb (11 contigs; Table S3). For
561 the *D. flavomontana* chromosome-level reference genome, the X chromosome (29.0Mb) could not be
562 further scaffolded, while the lengths of all other chromosomes increased due to scaffolding.
563 Chromosome 2L increased from 10.2Mb to 20.4Mb in length (3 contigs), 2R from 10.4Mb to 10.6Mb (3
564 contigs), the 3rd chromosome from 7.8Mb to 24.5Mb (33 contigs), the 4th chromosome from 20.0Mb
565 to 30.7Mb (14 contigs), and the 5th chromosome from 23.5Mb to 27.2Mb (4 contigs; Table S3).

566 Genome annotations

567 All genome assemblies were annotated for repetitive regions and genes. *De novo* libraries of repeat
568 sequences were built for each assembly using RepeatModeler v2.0.1 (Flynn et al. 2019), and repetitive
569 regions were softmasked – together with *Drosophila*-specific repeats (Dfam_3.1 (Hubley et al. 2016)
570 and RepBase-20181026 (Bao et al. 2015) – using RepeatMasker v4.1.0 (Smit *et al*. 2013-2015). Gene
571 models were predicted on the softmasked assemblies of *D. montana* using the BRAKER2 pipeline. For

572 gene annotation, we used RNA-seq data (Illumina Truseq 150bp PE) from whole-body female and male
573 *D. montana* adult flies collected in Finland (Parker et al. 2021). RNA-seq reads were trimmed for adapter
574 contamination and read quality using fastp v0.20.0 (Chen et al. 2018), and mapped to both softmasked
575 *D. montana* assemblies using STAR v2.7.0 (Dobin et al. 2013). Finally, *D. montana* gene annotations
576 were carried out with BRAKER2s ab initio gene prediction pipeline with RNA-seq and protein evidence
577 using Augustus v3.3.3 and GeneMark-ET v4.48 (Stanke et al. 2006; Stanke et al. 2008; Li et al. 2009;
578 Barnett et al. 2011; Lomsadze et al. 2014; Hoff et al. 2016; Hoff et al. 2019). Protein predictions of the
579 Jackson *D. montana* assembly with the best BUSCO values (see the Results) were used to annotate all
580 *D. flavomontana* genomes using the BRAKER2s ab initio gene prediction pipeline with GenomeThreader
581 and AUGUSTUS (Stanke et al. 2006; Stanke et al. 2008; Gremme 2013; Buchfink et al. 2015; Hoff et al.
582 2016; Hoff et al. 2019). Annotation completeness was assessed using BUSCO v5.1.2 against the
583 'diptera_odb10' database (Seppey *et al.* 2019).

584 Mapping, variant calling and variant filtering

585 To investigate genome-wide variation in sympatric and allopatric populations of the species, we
586 mapped all Illumina samples to the chromosome-level *D. montana* assembly. We quality-checked
587 Illumina PE reads of each sample with FastQC v0.11.8 (Andrews 2010) and trimmed for adapter
588 contamination and low-quality bases using fastp v0.20.0 (Chen et al., 2018). We mapped each trimmed
589 Illumina sample against the genome using BWA mem v0.7.17 with read group information (Li and
590 Durbin 2009), sorted alignments with SAMtools v1.10 (Li et al. 2009) and marked PCR duplicates with
591 sambamba v0.7.0 (Tarasov et al. 2015). The resulting BAM-files were used for variant calling with
592 freebayes v1.3.1-dirty (Garrison and Marth 2012). Raw variants were processed with gIMble preprocess
593 (genome-wide IM blockwise likelihood estimation toolkit; (Laetsch et al. 2022)). In brief, non-SNP
594 variants were deconstructed into allelic primitives, where remaining non-SNPs were removed in
595 addition to any SNP variant within two bp of a non-SNP. Genotype calls of remaining SNP variants were
596 set to missing if any of the following assumptions was violated: i) sample depth (FMT/DP) between 8
597 and 2SD from the mean coverage, ii) read directionality placement balance (RPL>=1, RPR>=1), or iii)
598 read strand placement balance (SAF>=1, SAR>=1).

599 Principal component analysis of whole-genome and climatic data

600 To group Illumina samples according to their species and population type, we performed a principal
601 component analysis (PCA) on the filtered VCF-file, including all samples and chromosomes as well as
602 coding, intronic and intergenic SNPs, using PLINK v1.9 package ((Chang et al. 2015), www.cog-
603 genomics.org/plink/1.9/). The VCF-file was converted to PLINK's BED/BIM format and the PCA was run
604 with PLINK's --pca function.

605 We performed another PCA on the climatic factors at fly sampling sites to visualize the climatic variation
606 amongst sites. First, we downloaded climatic information from WorldClim database v2.1 2.5min spatial
607 resolution, dataset 1970-2000, http://www.worldclim.org, (Fick and Hijmans 2017)) using latitudinal
608 and longitudinal coordinates of each site (Table S1) and extracted 19 bioclimatic variables using the
609 "raster" package v2.8-19 ((Hijmans and Etten 2020), Table S5, Table S6). We then performed PCA on
610 the bioclimatic variables, describing temperature and humidity conditions in each site. We performed
611 the PCA using the "FactoMineR" package (Lê et al. 2008) in R v3.4.3 (R Core Team 2017) and R studio
612 v1.1.383.

613 Characterization of chromosomal inversions

614 We identified large (>500kb) alternatively fixed inversions between *D. montana* and *D. flavomontana*
615 using both long- and short-read data. First, we mapped PacBio reads of each sample against each of
616 the four assemblies using ngmlr v0.2.7 (Sedlazeck et al. 2018) and obtained structural variant (SV)
617 candidates from the SV identification software, Sniffles v1.0.12 (Sedlazeck et al. 2018). Second, we
618 mapped Illumina read pairs against each of the four assemblies as explained in the "Mapping, variant

calling and variant filtering" paragraph. The resulting BAM-files were given to Delly v0.8.1, which identifies structural variants based on paired-end read orientation and split-read evidence (Rausch et al. 2012). Third, we used SURVIVOR (Jeffares et al. 2017) to identify species-specific, widespread inversions that were shared by Sniffles and Delly outputs and that are found in at least in 9 *D. montana* (out of 12) and 6 *D. flavomontana* (out of 9) samples. Putative breakpoints of each inversion were located within a single contig, except for the 4th chromosome inversion where breakpoints were located in two different contigs (Table S9). This inversion was therefore verified by mapping long- and short-read data against the *D. lummei* genome which has a more contiguous chromosome 4 (Table S9). The putative breakpoints of all inversions were confirmed visually with Integrative Genomics Viewer (IGV) v2.8.0 (Thorvaldsdóttir et al. 2012) using both long- and short-read data (Example of the IGV view shown in Fig. S9).

Modelling divergence and post-divergence gene flow

We analysed mean genetic divergence (d_{XY}) and fitted models of species' divergence with and without long-term interspecific gene flow between and within species using gIMble (Laetsch et al. 2022). This analytic likelihood method uses the joint distribution of mutation types in short sequence blocks, the blockwise site frequency spectrum (bSFS) across subsamples of pairs of individual genomes to fit a series of models of speciation history. We summarised data by the bSFS for two block lengths 64 bp and 128 bp.

To investigate the role of inversions in speciation, we fitted separate demographic models to inverted and colinear regions of the genome and to sympatric and allopatric comparisons of *D. montana* and *D. flavomontana*. Given the potentially different evolutionary history of the X chromosome and the autosomes (Vicoso and Charlesworth 2006; Charlesworth et al. 2018), we ran separate analyses for the X chromosome and autosomes. Colinear regions were combined across autosomes as these regions are expected to share the same evolutionary history, while inversions from different chromosomes may differ in age and were analysed separately. The overlapping inversions of the X chromosome were analysed together following Counterman and Noor (2006) and Lohse et al. (2015). We also analysed the split time of *D. montana* populations living in isolation (allopatry) and in contact (sympatry) with *D. flavomontana* to evaluate the timing of potential recent introgression between the two species. The intraspecific divergence time was inferred from the colinear autosomal regions, i.e. the same data partition we used to infer the interspecific background history.

We calculated d_{XY} for different genomic regions (i.e. colinear and inverted autosomes, and colinear and inverted X chromosome) and for allopatric and sympatric populations to evaluate the role of inversions in suppressing gene exchange. For a comparison, d_{XY} was also analysed for the intraspecific comparisons of *D. montana* (Fig. 1). These analyses were carried out separately for coding, intronic and intergenic regions (repetitive regions were excluded from all data partitions). To test whether genetic divergence was reduced within inversions, we simulated data sets corresponding in size to the data sampled for each inversion under the background demography (inferred from colinear autosomal regions) and compared the observed d_{XY} to the distribution. We simulated inversion datasets under a minimal, conservative model of recombination, which allows for gene conversion but no cross-over. We assumed a rate of (initiation of) gene conversion of 3.59×10^{-8} per bp per generation. This corresponds to recent estimates for *Drosophila pseudoobscura* and *Drosophila persimilis* (1.4×10^{-5} converted sites per bp per generation; mean GC tract length of 390 bp) (Korunes and Noor 2018) and simulated sequences of length 100kb, two orders of magnitude shorter than total length of intergenic sequence per inversion.

To investigate the speciation process of *D. flavomontana* and *D. montana*, we compared the fit of different demographic models. We limited the initial model selection of allopatric, sympatric and intraspecific comparisons to intergenic data of colinear autosomal regions (repetitive regions excluded) to minimize the effects of selection. The simplest, strict divergence (DIV) model considers isolation at time *T* without interspecific gene flow, i.e. isolation in allopatry (Fig. 7A). The isolation with migration (IM) model allows unidirectional migration rate at a constant rate *M* (Fig. 7B). The IM model was fitted

for both gene flow directions (i.e. from *D. montana* to *D. flavomontana* and from *D. flavomontana* to *D. montana*, and from allopatric to sympatric *D. montana* and from sympatric to allopatric *D. montana*). The DIV and IM models allow asymmetric effective population size (N_e) between the descendent populations, and the possibility of a separate N_e for the ancestral population. Analyses based on the bSFS assume a constant mutation rate (μ) across blocks and no recombination within them. We assumed a mutation rate (μ) of 2.8×10^{-9} per site per generation, based on an estimate of the spontaneous mutation rate in *Drosophila melanogaster* (Keightley et al. 2014). The estimates of *T* are converted into absolute time using $t = T \times 2N_e \times g$, where $N_e = \theta/(4\mu)$ and g is generation time. We assumed one generation per year, the generation time of Alaskan *D. montana* populations and most likely that of the ancestral population of the species, even though other *D. flavomontana* and *D. montana* populations presently have two generations per year (Tyukmaeva et al. 2020). To consider the potential effects of reference bias, we performed model fitting and selection twice using both *D. montana* and *D. flavomontana* chromosome-level assemblies as reference genomes.

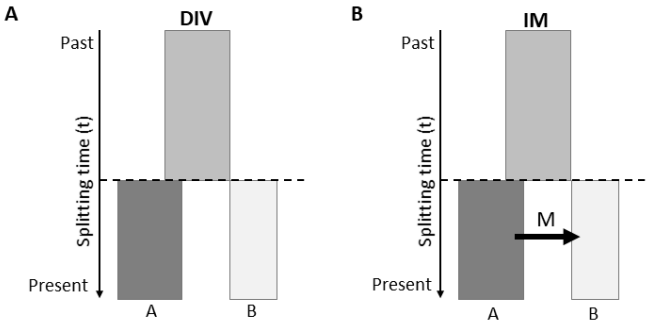

Figure 7. Sketches of the demographic models. The block widths indicate relative effective sizes (N_e) of the ancestral population and its two descendants A and B. (A) This model assumes no gene flow, i.e. strictly allopatric speciation (Div). (B) The isolation with migration IM) model allows unidirectional gene flow at rate *M* migrants per generation in this case from population A to B.

To estimate the uncertainty in parameter estimates, i.e. the difference in support (ΔlnCL) between different demographic scenarios, we performed a parametric bootstrap. We used gIMble simulate to simulate 100 replicate datasets (of the same size as the real data in terms of numbers of blocks). To include the effect of linkage between blocks, we simulated data in 1000 chunks assuming a recombination rate of 8.9×10^{-9} calculated from the total map length (i.e. 1.76×10^{-8} divided by two given the absence of recombination in males). Specifically, we simulated data under the best fitting DIV model and fitted that model and an IM model to each replicate to obtain a null distribution of ΔlnCL between models.

Finally, we performed demographic analyses under the best-fit models separately for different genomic partitions (i.e. colinear and inverted autosomes, and colinear and inverted X chromosome) and for allopatric and sympatric comparisons. The uncertainty in estimates of T and M for each data partition were inferred from 100 parametric bootstrap replicates/simulations. Parameter estimates from simulated datasets were analysed using a generalized linear model with Gamma (T, M) or Gaussian (M) distribution, depending on the normality of the data, in R. Here, colinear regions were compared to the inverted regions separately for autosomes and the X chromosome and for allopatric and sympatric populations, and estimates of M were compared between allopatric and sympatric populations within each chromosomal region.

Acknowledgements

We want to thank Anna-Lotta Hiillos and Jesse Mänttäri for their help with laboratory work and Edinburgh Genomics, Norwegian Sequencing Centre and BGI for sequencing the samples. This work was supported by the grant from Academy of Finland project 322980 to MK, and grant from Suomen Kulttuurirahasto (Keski-Suomen rahasto) to NP and MK. KL and DRL are supported by an ERC starting grant (ModelGenomLand, 757648). KL was also supported by a Natural Environmental Research Council (NERC) UK Independent Research fellowship (NE/L011522/1).

Author notes

K.L., M.K. and N.P. designed the study. N.P. carried out the DNA extractions and conducted the genome analyses with input from K.L. and D.R.L. K.L. designed and coded the simulations for d_{XY} analyses. M.K. supervised the laboratory work and funded the study. N.P. drafted the manuscript and all the authors helped in finalizing it.

Data accessibility

Raw reads of PacBio and Illumina samples as well as genome assemblies generated from the raw reads will be deposited on SRA at the time of publication.

References

Alonge M, Soyk S, Ramakrishnan S, Wang X, Goodwin S, Sedlazeck FJ, Lippman ZB, Schatz MC. 2019. RaGOO: fast and accurate reference-guided scaffolding of draft genomes. *Genome Biol.* 20:1–17.

Bao W, Kojima KK, Kohany O. 2015. Repbase Update, a database of repetitive elements in eukaryotic genomes. *Mob. DNA* [Internet] 6:4–9. Available from: http://dx.doi.org/10.1186/s13100-015-0041-9

Barb JG, Bowers JE, Renaut S, Rey JI, Knapp SJ, Rieseberg LH, Burke JM. 2014. Chromosomal evolution and patterns of introgression in *Helianthus*. *Genetics* 197:969–979.

Barnett DW, Garrison EK, Quinlan AR, Stŕmberg MP, Marth GT. 2011. Bamtools: A C++ API and toolkit for analyzing and managing BAM files. *Bioinformatics* 27:1691–1692.

Basset P, Yannic G, Brünner H, Hausser J. 2006. Restricted gene flow at specific parts of the shrew genome in chromosomal hybrid zones. *Evolution (N. Y).* 60:1718–1730.

Buchfink B, Xie C, Huson DH. 2015. Fast and sensitive protein alignment using DIAMOND. *Nat. Methods* 12:59–60.

Butlin RK. 2005. Recombination and speciation. *Mol. Ecol.* 14:2621–2635.

Camacho C, Coulouris G, Avagyan V, Ma N, Papadopoulos J, Bealer K, Madden TL. 2009. BLAST+: architecture and applications. *BMC Bioinformatics* 9:1–9.

Chakraborty M, Baldwin-Brown JG, Long AD, Emerson JJ. 2016. Contiguous and accurate de novo assembly of metazoan genomes with modest long read coverage. *Nucleic Acids Res.* 44:1–12.

Chang CC, Chow CC, Tellier LCAM, Vattikuti S, Purcell SM, Lee JJ. 2015. Second-generation PLINK: rising to the challenge of larger and richer datasets. *Gigascience* 4:s13742-015.

Charlesworth B, Campos JL, Jackson BC. 2018. Faster-X evolution: theory and evidence from *Drosophila*. *Mol. Ecol.* 27:3753–3771.

Charlesworth B, Coyne JA, Barton NH. 1987. The relative rates of evolution of sex chromosomes and autosomes. *Am. Nat.* 130:113–146.

Chen S, Zhou Y, Chen Y, Gu J. 2018. Fastp: An ultra-fast all-in-one FASTQ preprocessor. *Bioinformatics* 34:i884–i890.

Connallon T, Olito C, Dutoit L, Papoli H, Ruzicka F, Yong L. 2018. Local adaptation and the evolution of inversions on sex chromosomes and autosomes. *Philos. Trans. R. Soc. B Biol. Sci.* 373:20170423.

Counterman BA, Noor MAF. 2006. Multilocus test for introgression between the cactophilic species *Drosophila mojavensis* and *Drosophila arizonae*. *Am. Nat.* 168:682–696.

Cruickshank TE, Hahn MW. 2014. Reanalysis suggests that genomic islands of speciation are due to reduced diversity, not reduced gene flow. *Mol. Ecol.* 23:3133–3157.

Dobin A, Davis CA, Schlesinger F, Drenkow J, Zaleski C, Jha S, Batut P, Chaisson M, Gingeras TR. 2013. STAR: Ultrafast universal RNA-seq aligner. *Bioinformatics* 29:15–21.

Fang Z, Pyhäjärvi T, Weber AL, Dawe RK, Glaubitz JC, Jesus J De, González S, Ross-ibarra C, Doebley J, Morrell PL. 2012. Megabase-scale inversion polymorphism in the wild ancestor of maize. *Genetics* 191:883–894.

Faria R, Johannesson K, Butlin RK, Westram AM. 2018. Evolving Inversions. *Trends Ecol. Evol.* [Internet]:1–10. Available from: https://doi.org/10.1016/j.tree.2018.12.005

Faria R, Navarro A. 2010. Chromosomal speciation revisited: rearranging theory with pieces of evidence. *Trends Ecol. Evol.* [Internet] 25:660–669. Available from: http://dx.doi.org/10.1016/j.tree.2010.07.008

Felsenstein J. 2005. PHYLIP (Phylogeny Inference Package) version 3.6. Distributed by the author. Department of Genome Sciences, University of Washington, Seattle.

Fick SE, Hijmans RJ. 2017. WorldClim 2: new 1-km spatial resolution climate surfaces for global land areas. *Int. J. Climatol.* 37:4302–4315.

Fishman L, Stathos A, Beardsley PM, Williams CF, Hill JP. 2013. Chromosomal rearrangements and the genetics of reproductive barriers in *Mimulus* (monkeyflowers). *Evolution (N. Y).* 67:2547–2560.

Flynn JM, Hubley R, Goubert C, Rosen J, Clark AG, Feschotte C, Snit AF. 2019. RepeatModeler2: automated genomic discovery of transposable element families. *bioRxiv*:1–24.

Fuller ZL, Koury SA, Phadnis N, Chaeffer SW. 2019. How chromosomal rearrangements shape adaptation and speciation: Case studies in *Drosophila pseudoobscura* and its sibling species *Drosophila persimilis*. *Mol. Ecol.* 28:1283–1301.

Fuller ZL, Leonard CJ, Young RE, Schaeffer SW, Phadnis N. 2018. Ancestral polymorphisms explain the role of chromosomal inversions in speciation. *PLoS Genet.* 14:1–26.

Garrison E, Marth G. 2012. Haplotype-based variant detection from short-read sequencing. *arXiv Prepr. arXiv*:1207.3907 [q-bio.GN].

Gremme G. 2013. Computational Gene Structure Prediction.

774 Guan D, Mccarthy SA, Wang Y, Durbin R, Wood J, Howe K. 2020. Identifying and removing haplotypic duplication
775 in primary genome assemblies. *Bioinformatics* 36:2896–2898.
776 Guerrero RF, Rousset F, Kirkpatrick M. 2012. Coalescent patterns for chromosomal inversions in divergent
777 populations. *Philos. Trans. R. Soc. B Biol. Sci.* 367:430–438.
778 Halligan DL, Keightley PD. 2006. Ubiquitous selective constraints in the *Drosophila* genome revealed by a
779 genome-wide interspecies comparison. *Genome Res.* 16:875–884.
780 Harrison RG, Larson EL. 2014. Hybridization, introgression, and the nature of species boundaries. *J. Hered.*
781 105:795–809.
782 Hijmans RJ, Etten J Van. 2020. raster: Geographic data analysis and modeling. R package version 2.8-19.
783 Hoff KJ, Lange S, Lomsadze A, Borodovsky M, Stanke M. 2016. BRAKER1: Unsupervised RNA-Seq-Based Genome
784 Annotation with GeneMark-ET and AUGUSTUS. *Bioinformatics* 32:767–769.
785 Hoff KJ, Lomsadze A, Borodovsky M, Stanke M. 2019. Whole-genome annotation with BRAKER. *Methods Mol.*
786 *Biol.* 1962:65–95.
787 Hoffmann AA, Rieseberg LH. 2008. The of impact revisiting in evolution: inversions from genetic population
788 markers to drivers of adaptive shifts and speciation? *Annu. Rev. Ecol. Evol. Syst.* 39:21–42.
789 Hoikkala A, Poikela N. 2022. Adaptation and ecological speciation in seasonally varying environments at high
790 latitudes: *Drosophila virilis* group . *Fly (Austin).* [Internet] 16:85–104. Available from:
791 https://doi.org/10.1080/19336934.2021.2016327
792 Hopkins DP, Tyukmaeva VI, Gompert Z, Feder J, Nosil P. 2020. Functional genomics offers new tests of
793 speciation hypotheses. *Trends Ecol. Evol.* [Internet] 35:968–971. Available from:
794 https://doi.org/10.1016/j.tree.2020.08.001
795 Hubley R, Finn RD, Clements J, Eddy SR, Jones TA, Bao W, Smit AFA, Wheeler TJ. 2016. The Dfam database of
796 repetitive DNA families. *Nucleic Acids Res.* 44:D81–D89.
797 Jeffares DC, Jolly C, Hoti M, Speed D, Shaw L, Rallis C, Sedlazeck FJ. 2017. Transient structural variations have
798 strong effects on quantitative traits and reproductive isolation in fission yeast. *Nat. Commun.* 8:1–11.
799 Kapun M, Flatt T. 2018. The adaptive significance of chromosomal inversion polymorphisms in *Drosophila*
800 *melanogaster*. *Mol. Ecol.* 28:1263–1282.
801 Kapun M, Schmidt C, Durmaz E, Schmidt PS, Flatt T. 2016. Parallel effects of the inversion In(3R)Payne on body
802 size across the North American and Australian clines in *Drosophila melanogaster*. *J. Evol. Biol.* 29:1059–
803 1072.
804 Keightley PD, Ness RW, Halligan DL, Haddrill PR. 2014. Estimation of the spontaneous mutation rate per
805 nucleotide site in a *Drosophila melanogaster* full-sib family. *Genetics* 196:313–320.
806 Kirkpatrick M, Barton N. 2006. Chromosome inversions, local adaptation and speciation. *Genetics* 434:419–434.
807 Korunes KL, Noor MAF. 2018. Pervasive gene conversion in chromosomal inversion heterozygotes. *Mol. Ecol.*:1–
808 14.
809 Kulathinal RJ, Stevison LS, Noor MAF. 2009. The genomics of speciation in *Drosophila*: diversity, divergence, and
810 introgression estimated using low-coverage genome sequencing. *PLoS Genet.* 5:e1000550.
811 Laetsch DR, Bisschop G, Martin SH, Aeschbacher S, Lohse K. 2022. Demographically explicit scans for barriers to
812 gene flow using gIMble. *bioRxiv*:https://doi.org/10.1101/2022.10.27.514110.
813 Laetsch DR, Blaxter ML. 2017. BlobTools: Interrogation of genome assemblies. *F1000Research 2017* 6:1–16.
814 Lê S, Josse J, Husson F. 2008. FactoMineR: an R Package for multivariate analysis. *J. Stat. Softw.* 25:1–18.
815 Li H. 2018. Minimap2: pairwise alignment for nucleotide sequences. *Bioinformatics* 34:3094–3100.
816 Li H, Durbin R. 2009. Fast and accurate short read alignment with Burrows – Wheeler transform. *Bioinformatics*
817 25:1754–1760.
818 Li H, Handsaker B, Wysoker A, Fennell T, Ruan J, Homer N, Marth G, Abecasis G, Durbin R. 2009. The Sequence
819 Alignment / Map (SAM) Format and SAMtools. *Bioinformatics* 25:2078–2079.
820 Lohse K, Clarke M, Ritchie MG, Etges WJ. 2015. Genome-wide tests for introgression between cactophilic
821 *Drosophila* implicate a role of inversions during speciation. *Evolution* 69:1178–1190.
822 Lomsadze A, Burns PD, Borodovsky M. 2014. Integration of mapped RNA-Seq reads into automatic training of
823 eukaryotic gene finding algorithm. *Nucleic Acids Res.* 42:1–8.
824 Lowry DB, Willis JH. 2010. A widespread chromosomal inversion polymorphism contributes to a major life-
825 history transition, local adaptation, and reproductive isolation. *PLoS Biol.* 8.
826 Matzkin LM, Merritt TJS, Zhu C, Eanes WF. 2005. The structure and population genetics of the breakpoints
827 associated with the cosmopolitan chromosomal inversion In(3R)Payne in *Drosophila melanogaster*.
828 *Genetics* 170:1143–1152.
829 Michel AP, Grushko O, Guelbeogo WM, Lobo NF, Sagnon NF, Costantini C, Besansky NJ. 2006. Divergence with
830 gene flow in *Anopheles funestus* from the Sudan savanna of Burkina Faso, West Africa. *Genetics*

173:1389–1395.
Miller DE, Staber C, Zeitlinger J, Hawley RS. 2018. Highly contiguous genome assemblies of 15 *Drosophila* species generated using Manopore sequencing. *G3 Genes, Genomes, Genet.* 8:3131–3141.
Navarro A, Barton NH. 2003. Accumulating postzygotic isolation genes in parapatry: a new twist on chromosomal speciation. *Evolution (N. Y).* 57:447–459.
Noor MAF, Bennett SM. 2009. Islands of speciation or mirages in the desert? Examining the role of restricted recombination in maintaining species. *Heredity (Edinb).* 103:439–444.
Noor MAF, Garfield DA, Schaeffer SW, Machado CA. 2007. Divergence between the *Drosophila pseudoobscura* and *D. persimilis* genome sequences in relation to chromosomal inversions. *Genetics* 177:1417–1428.
Noor MAF, Grams KL, Bertucci LA, Reiland J. 2001. Chromosomal inversions and the reproductive isolation of species. *Proc. Natl. Acad. Sci. U. S. A.* 98:12084–12088.
Parker DJ, Envall T, Ritchie MG, Kankare M. 2021. Sex-specific responses to cold in a very cold-tolerant, northern *Drosophila* species. *Heredity (Edinb).* [Internet] 126:695–705. Available from: http://dx.doi.org/10.1038/s41437-020-00398-2
Parker DJ, Wiberg RAW, Trivedi U, Tyukmaeva VI, Gharbi K, Butlin RK, Hoikkala A, Kankare M, Ritchie MG. 2018. Inter and intraspecific genomic divergence in *Drosophila montana* shows evidence for cold adaptation. *Genome Biol. Evol.* 10:2086–2101.
Patterson JT. 1952. Revision of the *montana* complex of the *virilis* species group. *Univerisity Texas Publ.* 5204:20–34.
Poikela N, Kinnunen J, Wurdack M, Kauranen H, Schmitt T, Kankare M, Snook RR, Hoikkala A. 2019. Strength of sexual and postmating prezygotic barriers varies between sympatric populations with different histories and species abundances. *Evolution (N. Y).* 73:1182–1199.
Poikela N, Laetsch DR, Kankare M, Hoikkala A, Lohse K. 2022. Experimental introgression in *Drosophila*: asymmetric postzygotic isolation associated with chromosomal inversions and an incompatibility locus on the X chromosome. *bioRxiv*:1–17.
Poikela N, Tyukmaeva V, Hoikkala A, Kankare M. 2021. Multiple paths to cold tolerance: the role of environmental cues, morphological traits and the circadian clock gene *vrille*. *BMC Ecol. Evol.* [Internet] 21:1–20. Available from: https://doi.org/10.1186/s12862-021-01849-y
Rausch T, Zichner T, Schlattl A, Stütz AM, Benes V, Korbel JO. 2012. DELLY: structural variant discovery by integrated paired-end and split-read analysis. *Bioinformatics* 28:333–339.
Ruan J, Li H. 2020. Fast and accurate long-read assembly with wtdbg2. *Nat. Methods* 17:155–158.
Schäfer MA, Mazzi D, Klappert K, Kauranen H, Vieira J, Hoikkala A, Ritchie MG, Schlötterer C. 2010. A microsatellite linkage map for *Drosophila montana* shows large variation in recombination rates, and a courtship song trait maps to an area of low recombination. *J. Evol. Biol.* 23:518–527.
Sedlazeck FJ, Rescheneder P, Smolka M, Fang H, Nattestad M, Haeseler A Von, Schatz MC. 2018. Accurate detection of complex structural variations using single-molecule sequencing. *Nat. Methods* [Internet] 15:461–468. Available from: http://dx.doi.org/10.1038/s41592-018-0001-7
Seehausen O, Butlin RK, Keller I, Wagner CE, Boughman JW, Hohenlohe PA, Peichel CL, Saetre GP, Bank C, Brännström Å, et al. 2014. Genomics and the origin of species. *Nat. Rev. Genet.* 15:176–192.
Seppey M, Manni M, Zdobnov EM. 2019. BUSCO: assessing genome assembly and annotation completeness. *In Gene prediction* (pp. 227-245). Humana, New York, NY.
Servedio MR, Noor MAF. 2003. The role of reinforcement in speciation: theory and data. *Annu. Rev. Ecol. Evol. Syst.* [Internet] 34:339–364. Available from: http://www.jstor.org/stable/30033779%5Cnhttp://www.jstor.org/stable/30033779?seq=1&cid=pdf-reference#references_tab_contents%5Cnhttp://about.jstor.org/terms
Stanke M, Diekhans M, Baertsch R, Haussler D. 2008. Using native and syntenically mapped cDNA alignments to improve de novo gene finding. *Bioinformatics* 24:637–644.
Stanke M, Schöffmann O, Morgenstern B, Waack S. 2006. Gene prediction in eukaryotes with a generalized hidden Markov model that uses hints from external sources. *BMC Bioinformatics* 7:1–11.
Stone WS, Guest WC, Wilson FD. 1960. The evolutionary implications of the cytological polymorphism and phylogeny of the *virilis* group of *Drosophila*. *Proc. Natl. Acad. Sci.* 46:350–361.
Sturtevant AH. 1921. A case of rearrangement of genes in *Drosophila*. *Proc. Natl. Acad. Sci. U. S. A.* 7:235–237.
Tarasov A, Vilella AJ, Cuppen E, Nijman IJ, Prins P. 2015. Sambamba: fast processing of NGS alignment formats. *Bioinformatics* 31:2032–2034.
Thorvaldsdóttir H, Robinson JT, Mesirov JP. 2012. Integrative Genomics Viewer (IGV): high-performance genomics data visualization and exploration. *Brief. Bioinform.* 14:178–192.
Throckmorton LH. 1982. The *virilis* species group. *Genet. Bioogy Drosoph.* 3:227–296.

Trickett AJ, Butlin RK. 1994. Recombination suppressors and the evolution of new species. *Heredity (Edinb).* 73:339–345.

Tyukmaeva VI, Lankinen P, Kinnunen J, Kauranen H, Hoikkala A. 2020. Latitudinal clines in the timing and temperature-sensitivity of photoperiodic reproductive diapause in *Drosophila montana*. *Ecography (Cop.).* 43:1–10.

Vicoso B, Charlesworth B. 2006. Evolution on the X chromosome: unusual patterns and processes. *Nat. Rev. Genet.* 7:645–653.

Walker BJ, Abeel T, Shea T, Priest M, Abouelliel A, Sakthikumar S, Cuomo CA, Zeng Q, Wortman J, Young SK, et al. 2014. Pilon: An integrated tool for comprehensive microbial variant detection and genome assembly improvement. *PLoS One* 9.

Wallberg A, Schöning C, Webster MT, Hasselmann M. 2017. Two extended haplotype blocks are associated with adaptation to high altitude habitats in East African honey bees. *PLoS Genet.* 13:e1006792.

Wellenreuther M, Bernatchez L. 2018. Eco-evolutionary genomics of chromosomal inversions. *Trends Ecol. Evol.* [Internet] 33:427–440. Available from: http://dx.doi.org/10.1016/j.tree.2018.04.002

Wellenreuther M, Mérot C, Berdan E, Bernatchez L. 2019. Going beyond SNPs: The role of structural genomic variants in adaptive evolution and species diversification. *Mol. Ecol.* 28:1203–1209.

White NJ, Snook RR, Eyres I. 2020. The past and future of experimental speciation. *Trends Ecol. Evol.* [Internet] 35:10–21. Available from: https://doi.org/10.1016/j.tree.2019.08.009

Yang H, Jaime M, Polihronakis M, Kanegawa K, Markow T, Kaneshiro K, Oliver B. 2018. Re-annotation of eight *Drosophila* genomes. *Life Sci. alliance* 1:1–14.

Yusuf L, Tyukmaeave V, Hoikkala A, Ritchie M. 2022. Divergence and introgression among the *virilis* group of *Drosophila*. *bioRxiv*:https://doi.org/10.1101/2022.01.11.475832.

Zimin A V, Puiu D, Luo M, Zhu T, Koren S, Marçais G, Yorke JA, Dvor J, Salzberg SL. 2017. Hybrid assembly of the large and highly repetitive genome of Aegilops tauschii, a progenitor of bread wheat, with the MaSuRCA mega-reads algorithm. *Genome Res.* 27:787–792.